

Control Interaction of Two PV power plants with Volt - Var Control

S. Mohan, R.K. Varma
Department of Electrical and Computer Engineering,
The University of Western Ontario,
Canada.

SUMMARY

The potential of adverse control interaction among multiple smart PV inverters located in close vicinity is becoming a concern for utilities given the significant growth of PV systems worldwide. This paper provides a comprehensive stability analysis of two adjacent PV plants in a realistic utility distribution feeder considering the impact of various factors, and provides insights into the selection of appropriate settings for stable operation of neighbouring PV plants under diverse operating conditions.

Volt-Var control is one of the widely implemented smart inverter function for voltage control, which is mandated by recent Standards and Grid codes such as IEEE 1547 -2018, California Rule 21, etc. Different studies of control interactions of smart inverters with volt-var control are reported in literature with seemingly divergent conclusions in some cases. Some studies have reported that the interaction between adjacent PV plants can be minimized by increasing the controller delay, whereas other studies have reported the opposite. This provided the motivation to perform a wide-ranging study to encompass the results of all the previously reported cases.

A detailed small signal model of two PV plants connected to a realistic 45 km long 27.6 kV feeder in Ontario is developed in this paper. The developed model considers network dynamics, load dynamics, and PV plant dynamics (inverter, LCL filter, controllers and associated measurement filters, and coupling transformer). The different components are modelled as submodules on their own rotating frame and are transformed to a common $d-q$ reference frame to obtain the complete system model.

The impact of slope of Volt-Var function, delay (includes voltage averaging time, and other inherent delays in voltage control loop), response time of current controller, distance between PV plants, and X/R ratio of feeder, on the controller interaction are investigated. The results of small signal studies are subsequently validated by time domain simulations. This work presents a comprehensive evaluation and thus provides valuable insights on the interaction between multiple PV plants while providing Volt-Var control. Additionally, it also bridges the different perspectives reported in literature on impact of delay on interaction between two PV plants.

KEYWORDS

Volt-Var, PV solar systems, Control Interaction, Smart Inverter, Advanced inverters, Voltage Control, Reactive power control, Distributed Energy Resources

Corresponding author: rkvarma@uwo.ca

I. INTRODUCTION

With increasing concern over global warming, the use of renewable energy is growing at a rapid rate around the world [1]. It is predicted that the global installed capacity of PV systems will reach 1100 GW by 2023 [2]. As conventional centralized thermal generators are replaced with distributed renewable energy sources such as solar photovoltaic, it leads to overvoltage issues in the distribution system. To improve the voltage quality at distribution network, advanced Photovoltaic (PV) inverters are required to provide control of real and reactive power both autonomously as well as in response to utility communicated signals [3]. These advanced inverters termed as smart inverters provide different grid support functions including Volt/Var control, Volt/Watt control, Frequency/Watt control, ramp rate control, High/Low Voltage Ride Through (H/L VRT), High/Low-Frequency Ride Through (H/L FRT), etc. [3], [4].

Volt-Var control is one of the widely implemented smart inverter functions for voltage control, which is mandated by recent Standards and Grid codes such as IEEE 1547 -2018 [5], California Rule 21 [6], etc. With the rapidly growing proliferation of PV power plants in electrical networks, it is highly likely that multiple PV plants (up to few MW) may get connected to the same distribution feeder. The participation of multiple neighboring PV units in voltage regulation may cause excessive circulating current between PV inverters, or even unstable operation of the PV inverters. The possibility of these potential adverse control interactions between multiple smart inverters is becoming a concern for utilities. These interactions are influenced by the inverter response time, slope of Volt-Var function, delay, and distribution feeder parameters. Even though the impact of above factors on control interactions are reported in literature [7-10], no comprehensive analysis considering all the above said parameters are reported to the best of authors' knowledge. Furthermore, different studies on the impact of time delay on control interactions of smart inverters with Volt-Var control reported seemingly divergent conclusions. The studies in [7-9] reported that an increase in controller delay causes undesirable oscillations whereas [10] reported the opposite. These reasons provided the motivation to perform a wide-ranging study to encompass the results of all the previously reported cases.

This paper presents a comprehensive evaluation of control interactions between two PV plants while providing Volt-Var control using a detailed system model considering PV plant dynamics, load dynamics, and network dynamics. The novel contributions of this paper are that it:

- provides insights on the impact of various PV plant, and distribution system parameters on interaction between multiple PV plants while providing Volt-Var control.
- bridges the different perspectives reported in the literature on the impact of delay on the interaction between two PV plants.

The rest of the paper is organized as follows. The study system is described in section II, whereas the small-signal model is presented in section III. The results of small-signal analysis and time-domain simulation studies are shown in section IV, and V, respectively. The conclusion of this work is stated in section VI.

II. STUDY SYSTEM

The study system is illustrated in Figure 1. It is adapted from a 45 km long 27.6 kV feeder in Ontario, Canada [11]. The feeder is energized by 115kV transmission network and it is transformed to 27.6 kV by the transformer T_1 at distribution substation. Two PV plants of 6 MW ratings are connected to the feeder at Bus 2, which are 35 km away from the distribution substation. Total load (SL) of 5.3 MVA at 0.9 power factor is connected at feeder end. Each PV plant consists of DC link capacitor, inverter, LCL filter, padmount transformer, and collector cables. The MPPT voltage is assumed to be 1.2 kV in this study. The LCL filter is designed as per [12]. The padmount transformer T_2 is rated at 0.480/27.6 kV. The HV terminal of T_2 is considered as PoC for the PV plant. The PV power is fed to the distribution feeder through collector cables[13]. Bus 2 is the PCC for both PV plants.

III. SMALL SIGNAL MODELING OF STUDY SYSTEM

The small signal model of the study system is developed in synchronously rotating $d-q$ frame. The modeling strategy used is dividing study system into multiple sub modules and modeling each submodule in its corresponding $d-q$ frame. The state space equations of network components and the

load are derived on a $d-q$ frame (d_n, q_n) rotating at network frequency. This frame is considered as the common reference frame in this study. Each individual PV inverter is modelled on a $d-q$ frame (d_i, q_i), whose rotational frequency is set by the inverters phase locked loop. The inverter models in their individual $d-q$ frame (d_i, q_i) frame are then transformed to the common $d-q$ frame (d_n, q_n) using the transformation given in (1).

$$T = \begin{bmatrix} \cos \delta_i & -\sin \delta_i \\ \sin \delta_i & \cos \delta_i \end{bmatrix} \quad (1)$$

where, δ_i is the angle difference the rotational frame of i^{th} inverter (d_i, q_i) and network frame (d_n, q_n).

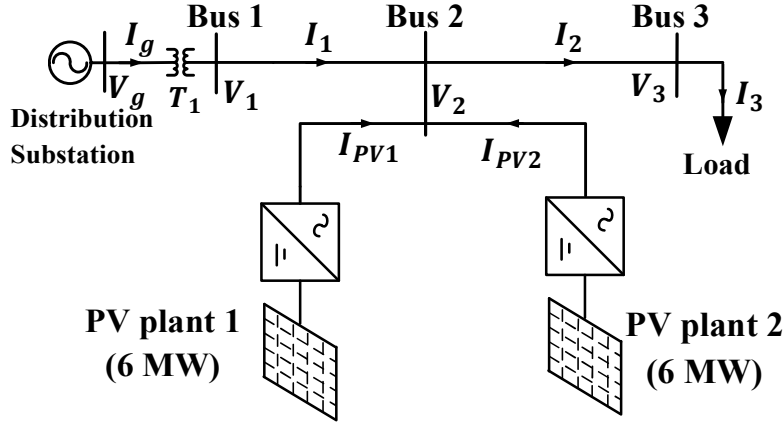


Figure 1. Single line diagram of study system.

A. Network Model

The network model consists of state space equations of 115kV transmission network, transformer T_1 , distribution feeder and load. The 115kV transmission network is modelled as a voltage source behind Thevenin's equivalent impedance. The distribution feeder is represented by its lumped π equivalent model. The load is modelled as constant impedance, resistive – inductive load. The state space model of the network developed in abc frame and are transformed to $d-q$ frame [14]. This model is then linearized around an operating point to obtain the state space model of the network. The small signal model of the network is given in (2).

$$\begin{aligned} \widetilde{\mathbf{X}}_n &= A_1 \widetilde{\mathbf{X}}_n + B_{11} \widetilde{\mathbf{U}}_{11} + B_{12} \widetilde{\mathbf{U}}_{12} + B_{13} \widetilde{\mathbf{U}}_{13} \\ \widetilde{\mathbf{Y}}_{11} &= C_{11} \widetilde{\mathbf{X}}_n \end{aligned} \quad (2)$$

where,

$$\begin{aligned} \widetilde{\mathbf{X}}_n &= [\widetilde{V}_{1d} \ \widetilde{V}_{1q} \ \widetilde{V}_{2d} \ \widetilde{V}_{2q} \ \widetilde{V}_{3d} \ \widetilde{V}_{3q} \ \widetilde{I}_{gd} \ \widetilde{I}_{gq} \ \widetilde{I}_{1d} \ \widetilde{I}_{1q} \ \widetilde{I}_{2d} \ \widetilde{I}_{2q} \ \widetilde{I}_{3d} \ \widetilde{I}_{3q}]^T \\ \widetilde{\mathbf{U}}_{11} &= [\widetilde{V}_{gd} \ \widetilde{V}_{gq}]^T, \widetilde{\mathbf{U}}_{12} = [\widetilde{I}_{PV1d} \ \widetilde{I}_{PV1q}]^T, \widetilde{\mathbf{U}}_{13} = [\widetilde{I}_{PV2d} \ \widetilde{I}_{PV2q}]^T \\ \widetilde{\mathbf{Y}}_{11} &= [\widetilde{V}_{2d} \ \widetilde{V}_{2q}]^T \end{aligned}$$

V_{jd} and V_{jq} are the $d-q$ components of j^{th} bus voltage. I_{jd} and I_{jq} are the $d-q$ components of current flowing through the feeder connecting j^{th} and $(j+1)^{\text{th}}$ bus. I_{gd} and I_{gq} are the $d-q$ components of grid current. V_{gd} and V_{gq} are the $d-q$ components of grid voltage. I_{PVjd} and I_{PVjq} are the $d-q$ components of output current of j^{th} PV solar farm.

A_1 is the system matrix. B_{11} , B_{12} and B_{13} are the control matrixes. C_{11} and C_{12} are the output matrixes. The variables with ' \sim ' represents linearized quantity. There are 14 states, 6 inputs and 4 outputs in the developed network model.

1) Model of a PV plant

The PV plant consists of two sub systems: PV power circuit and control circuit. PV power circuit consists of Voltage Source Converter (VSC), filter, pad mounting transformer, and collector cables. The control circuit includes Phase Locked Loop (PLL), current controllers, measurement filter, Volt-Var controller and Active power controller.

2) PV power circuit

The PV power circuit model consists of DC link capacitor, LC filter, padmount transformer, and collector cable dynamics [14]. The developed small signal model of the PV plant is given in (3).

$$\begin{aligned}\dot{\tilde{X}}_2 &= A_2\tilde{X}_2 + B_{21}\tilde{U}_{21} + B_{22}\tilde{U}_{22} \\ \tilde{Y}_{21} &= C_{21}\tilde{X}_2, \tilde{Y}_{22} = C_{22}\tilde{X}_2\end{aligned}\quad (3)$$

where,

$$\begin{aligned}\tilde{X}_2 &= [\tilde{V}_{dc} \quad \tilde{I}_{invd} \quad \tilde{I}_{invq} \quad \tilde{V}_{cfd} \quad \tilde{V}_{cfq} \quad \tilde{V}_{Pocd} \quad \tilde{V}_{Pocq} \quad \tilde{I}_{Pocd} \quad \tilde{I}_{Pocq} \quad \tilde{I}_{Pvd} \quad \tilde{I}_{Pvq}]^T \\ \tilde{U}_{21} &= [\tilde{V}_{PCCd} \quad \tilde{V}_{PCCq}]^T, \quad \tilde{U}_{22} = [\tilde{m}_d \quad \tilde{m}_q \quad \tilde{\omega}_{pv}]^T \\ \tilde{Y}_{21} &= [\tilde{I}_{Pvd} \quad \tilde{I}_{Pvq}]^T, \quad \tilde{Y}_{22} = [\tilde{V}_{dc} \quad \tilde{I}_{invd} \quad \tilde{I}_{invq} \quad \tilde{V}_{cfd} \quad \tilde{V}_{cfq} \quad \tilde{V}_{Pocd} \quad \tilde{V}_{Pocq}]^T\end{aligned}$$

V_{dc} is the DC link voltage. I_{invd} , I_{invq} , V_{cfd} , V_{cfq} , V_{Pocd} , V_{Pocq} , I_{Pocd} , I_{Pocq} , I_{Pvd} , I_{Pvq} , V_{PCCd} , V_{PCCq} , are d - q components of VSC output current, filter capacitor terminal voltage, PoC voltage, PoC current, PCC current, and PCC voltage, respectively.

3) PV control system

The modeling of Volt-Var controller is discussed below. The other controller components are modelled as per [15], and are not included here due to limitation of space. The structure of a typical Volt-Var controller is shown in Figure 2. The Volt-Var controller generates reactive power set point based on moving fixed width time window average value of PV terminal voltage. The moving average window time (denoted as delay here), dead band and slope of Volt-Var curve are user settable [3].

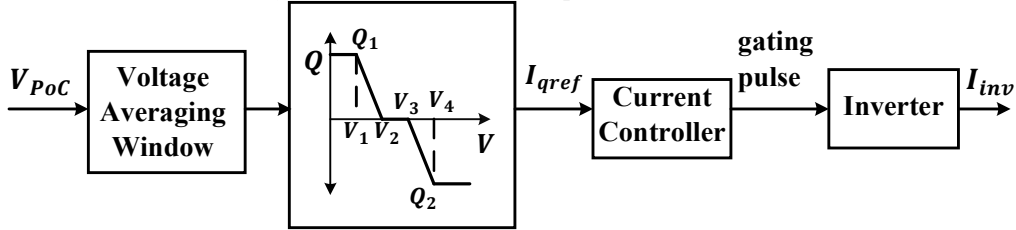


Figure 2. Structure of a Volt-Var controller.

The dynamics of Volt-Var controller are defined by (4).

$$\begin{aligned}\frac{dX_{vv}}{dt} &= \frac{V_{Poc}}{\tau_d} - \frac{X_{vv}}{\tau_d} \\ I_{qref} &= \frac{2*Slope_{ind}}{3V_{cfdm}} (X_{vv} - V_3), \text{ for Voltage swell.} \\ I_{qref} &= \frac{2*Slope_{cap}}{3V_{cfdm}} (X_{vv} - V_2), \text{ for Voltage sag.}\end{aligned}\quad (4)$$

where, $Slope_{ind}$ and $Slope_{cap}$ are the slopes of inductive and capacitive operations of Volt-Var curve. τ_d is the time constant of voltage averaging window. V_3 is the lowest voltage level for which inverter generates inductive reactive power. V_2 is the highest voltage level for which inverter generates capacitive reactive power. The calculation of I_{qref} is different for inductive (voltage swell), and capacitive (voltage sag) operation of Volt – Var control. Thus, while developing small signal model, appropriate equation for I_{qref} should be used based on mode of operation (capacitive or inductive). The small signal model of PV control system is given by (5).

$$\begin{aligned}\dot{\tilde{X}}_3 &= A_3\tilde{X}_3 + B_{31}\tilde{U}_{31} + B_{32}\tilde{U}_{32} \\ \tilde{Y}_{31} &= C_{31}\tilde{X}_3 + D_{31}\tilde{U}_{32}\end{aligned}\quad (5)$$

where,

$$\begin{aligned} \widetilde{X}_3 &= [\widetilde{V}_{PoCdm} \ \widetilde{V}_{PoCqm} \ \widetilde{V}_{cfdm} \ \widetilde{V}_{cfqm} \ \widetilde{X}_{pll} \ \widetilde{\rho}_{pv} \ \widetilde{X}_d \ \widetilde{X}_q \ \widetilde{X}_{dc} \ \widetilde{X}_{vv}]^T \\ \widetilde{U}_{31} &= [\widetilde{V}_{dc} \ \widetilde{I}_{invd} \ \widetilde{I}_{invq} \ \widetilde{V}_{cfd} \ \widetilde{V}_{cfq} \ \widetilde{V}_{PoCd} \ \widetilde{V}_{PoCq}]^T, \widetilde{U}_{32} = [\widetilde{V}_{dcref}] \\ \widetilde{Y}_{31} &= [\widetilde{m}_d \ \widetilde{m}_q \ \widetilde{\omega}_{pv}]^T \end{aligned}$$

$\widetilde{V}_{PoCdm}, \widetilde{V}_{PoCqm}, \widetilde{V}_{cfdm}, \widetilde{V}_{cfqm}$, are d - q components of filtered PoC voltage, and filter capacitor terminal voltage, respectively. $\widetilde{\rho}_{pv}, \widetilde{X}_{pll}, \widetilde{X}_d, \widetilde{X}_q, \widetilde{X}_{dc}$, and \widetilde{X}_{vv} , are PoC voltage angle, and state variables of PLL, d and q axis current controller, DC voltage controller, and Volt-Var controller, respectively. \widetilde{m}_d and \widetilde{m}_q are d and q axis components of modulation index respectively. \widetilde{V}_{dcref} is the DC link voltage reference.

4) Complete model of PV Plant.

The overall model of PV system is obtained by combining the models of PV power circuit (3) and PV control system (5), and expressed as (6). The model of each PV plant has 21 states, 3 inputs and 2 outputs.

$$\begin{aligned} \dot{\widetilde{X}}_{PVj} &= A_{PVj}\widetilde{X}_{PVj} + B_{PVj1}\widetilde{U}_{PVj1} + B_{PVj2}\widetilde{U}_{PVj2} \\ \widetilde{Y}_{PVj} &= C_{PVj}\widetilde{X}_{PVj} \end{aligned} \quad (6)$$

where,

$$\begin{aligned} A_{PVj} &= \begin{bmatrix} A_2 & B_{21}C_{31} \\ B_{31}C_{22} & A_3 \end{bmatrix}_{21 \times 21} \\ B_{PVj1} &= [B_{21}]_{21 \times 2}, \quad B_{PVj2} = [B_{32}]_{21 \times 1}, \quad C_{PVj} = [C_{21} \ 0]_{2 \times 21} \\ \widetilde{X}_{PVj} &= [\widetilde{X}_2 \ \widetilde{X}_3]^T, \quad \widetilde{U}_{PVj1} = [\widetilde{U}_{21}]^T = [\widetilde{V}_{po1d} \ \widetilde{V}_{po1q}]^T, \quad \widetilde{U}_{PVj2} = [\widetilde{U}_{32}] = [\widetilde{V}_{dcref}] \\ \widetilde{Y}_{PVj} &= [\widetilde{Y}_{21}]^T = [I_{PVd} \ I_{PVq}]^T \end{aligned}$$

subscript j denotes j^{th} PV plant.

B. Overall System Model

The linearized model of complete study system is obtained by combining the models of network (2), PV plant 1 and PV plant 2, as given in (7). Both PV plants are modelled using (6). The overall system model with two PV plants and network have 56 states and 4 inputs.

$$\dot{\widetilde{X}}_{sys} = A_{sys}\widetilde{X}_{sys} + B_{sys}\widetilde{U}_{sys} \quad (7)$$

where,

$$\begin{aligned} A_{sys} &= \begin{bmatrix} A_1 & B_{12}C_{PV1} & B_{13}C_{PV2} \\ B_{PV11}C_{11} & A_{PV1} & 0 \\ B_{PV21}C_{12} & 0 & A_{PV2} \end{bmatrix}_{56 \times 56} \\ B_{sys} &= \begin{bmatrix} B_{11} & 0 & 0 \\ 0 & B_{PV12} & 0 \\ 0 & 0 & B_{PV12} \end{bmatrix}_{56 \times 4} \\ \widetilde{X}_{sys} &= [\widetilde{X}_n \ \widetilde{X}_{PV1} \ \widetilde{X}_{PV2}]^T, \quad \widetilde{U}_{sys} = [\widetilde{V}_{gd} \ \widetilde{V}_{gq} \ \widetilde{V}_{dc1ref} \ \widetilde{V}_{dc2ref}]^T \end{aligned}$$

IV. SMALL SIGNAL STUDIES

The impact of variation of various parameters on control interaction between neighbouring PV plants while providing Volt-Var control is studied in this section. Both PV plants are assumed to be generating 0.9 pu active power and operating in inductive mode (Voltage swell) of Volt-Var control.

A. Impact of delay

The impact of time delay on control interaction is investigated by varying the delay between 0.001s - 1s. The response time and slope are set at 0.007s, and 15, respectively. The X/R of feeder and short circuit ratio at PCC are 2.5, and 3.5, respectively. The locus of dominant poles for the variation of delay are illustrated in Figure 3. With increase in delay, the dominant pole shift to right, and eventually make system unstable. However further increase in delay shifts the pole to left and thus making the system stable. This observation shows that increase in delay can have either a positive or negative impact on control interactions.

B. Impact of response time

The loci of dominant poles for variation of response time is studied by varying response time between 0.001s - 1s, and results are depicted in Figure 4. The delay and slope are 0.005s, and 15,

respectively. The X/R of feeder and short circuit ratio at PCC are 2.5, and 3.5, respectively. For the variation of response time, dominant pole shows similar behavior as in the case of variation of delay. The control interaction is minimal for the fastest response (small response time). The frequency of oscillation is high for the smallest response time (fastest control), but the oscillations damp fast due to large damping ratio. The frequency and damping ratio of the sensitive mode decreases with increase in response time, and the mode eventually becomes unstable. With further increase in response time, the sensitive mode shift towards left and becomes stable, again.

The above studies show that response time and delay have similar impact on control interactions. The increase in delay and response time can both positively or negatively damp the control interactions. Thus, based on the initial operating point and range of variation of these factors considered, different results can be obtained. This explains the different perspectives reported in literature on impact of delay and response time.

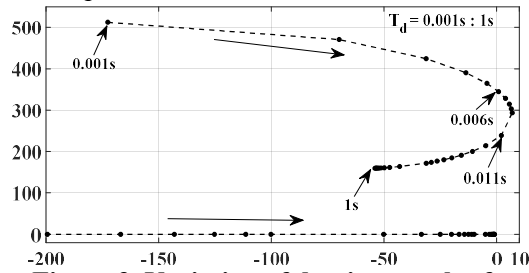


Figure 3. Variation of dominant poles for varying delay.

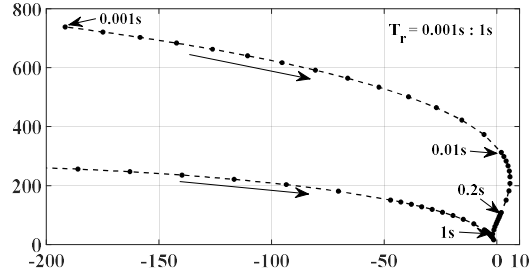


Figure 4. Variation of dominant poles for varying response time.

C. Impact of Slope

The effect of slope of Volt-Var controller on control interaction is studied by varying the slope between 5 - 40. The delay and response time are 0.008 s, and 0.003 s, respectively. The X/R of feeder and short circuit ratio at PCC are 2.5, and 3.5, respectively. The result of this study is illustrated in Figure 5. As the slope increases, the sensitive mode shifts right and thus reduces the stability of system. The reactive power injected by PV plant increases with increase in slope. For a large slope, the larger reactive power injection causes greater variation in voltage and potentially lead to oscillatory response. However, for small slope, the reactive power injected by PV plant is low. Hence, the variation in voltage is lesser compared to large slope, and a more stable response is obtained.

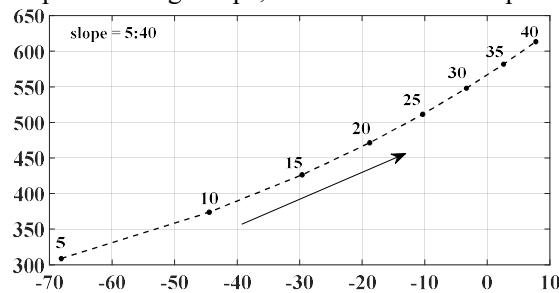


Figure 5. Variation of dominant poles for varying slope.

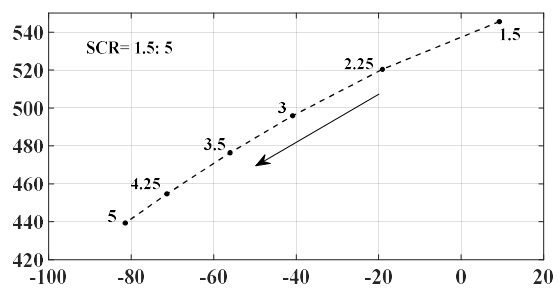


Figure 6. Variation of dominant poles for varying SCR.

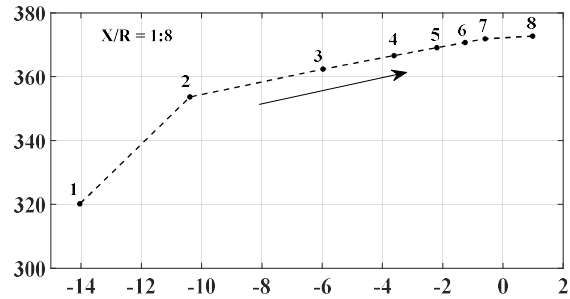


Figure 7. Variation of dominant poles for varying X/R.

D. Impact of System strength

The effect of system strength is evaluated by varying the short circuit ratio (SCR) at Bus 2 from 1.5 (weak system) to 5 (strong system), and the results are shown in Figure 6. The delay and response time are 0.008 s, and 0.003 s, respectively. The slope is 15. The X/R of feeder is 2.5. The sensitive mode shifts to the right with reduction in system strength. With decrease in system strength, the modal damping of sensitive mode reduces, whereas its frequency increases.

E. Impact of feeder X/R ratio

The system X/R is varied between 1-8 to study its influence on the interaction between PV plants while providing Volt-Var control. In this study, the delay and response time are 0.008s, and 0.006s, respectively. The slope is 15. The short circuit ratio at PCC is 3.5. The locus of dominant mode is plotted in Figure 7. With increasing X/R, as the network becomes more inductive, the sensitive pole shifts to the right. The control interaction is minimal in a network with low X/R ratio due to the large damping introduced by the higher resistance.

V. TIME DOMAIN SIMULATION STUDIES

Time domain simulation studies are done on PSCAD software to validate the results of small signal studies. In the following simulation studies, both PV plants are initially generating 0.9 pu active power at unity power factor (UPF). The Volt-Var control of PV plant 1 (PV1) and PV plant 2 (PV2) are enabled at 1.5s, and 2.5s, respectively. The system conditions are identical to small signal studies, with X/R, SCR and slope as 2.5, 3.5, and 15, respectively.

A. Impact of delay

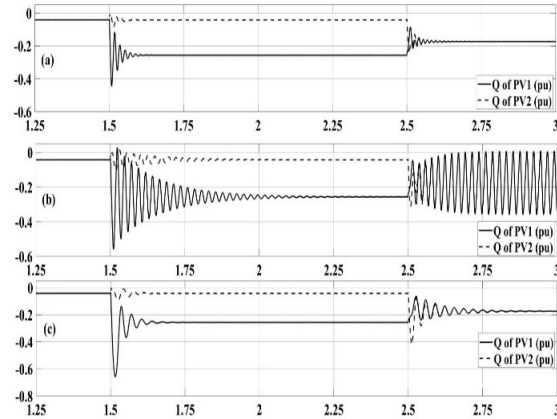


Figure 8. Reactive power output (Q) of both PV plants for delays of: (a) 0.003 s, (b) 0.009 s, and (c) 0.05 s.

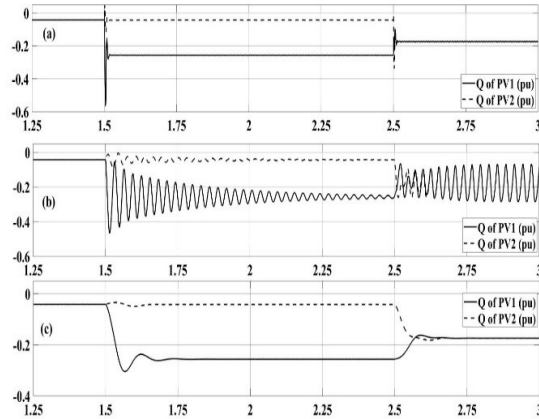


Figure 9. Reactive power output (Q) of both PV plants for response time of: (a) 0.001 s, (b) 0.015 s, and (c) 0.5 s.

The reactive power output (Q) of both PV plants for three different time delays are depicted in Figure 8. Figure 8 (a) - (c) depicts response for delays of 0.003 s, 0.009 s, and 0.05 s, respectively. The response time is 0.007 s for all the cases. The system is stable for small value of delay (0.003 s), and a large value of delay (0.05 s), whereas it is unstable for an intermediate value of delay (0.009 s). These results correlate well with the small signal analysis. These results further confirm that system becomes unstable with increase in delay, and a further increase in delay makes the system stable

B. Impact of response time

The reactive power output (Q) of both PV plants for three different response time are illustrated in Figure 9. Figure 9 (a) – (c) depicts reactive power for response times of 0.001 s, 0.015 s, and 0.5 s, respectively. The delay is 0.005 s. Stable response is observed for small response time (0.001 s), and large response time (0.5 s). But the system is unstable for intermediate value of response time (0.015 s). This result also matches with the small signal results.

The above time domain simulation verifies that the variation of delay or response time can cause either a stable or unstable response. Thus, to ensure stable operation, the impact of delay and response should be studied for the specific system before setting the above parameters.

VI. CONCLUSION

The Volt-Var control of neighbouring PV plants can potentially cause undesirable control interactions between them. With the rapid growth of PV plants, the possibility of these undesirable interactions is becoming a concern for utilities. In literature, apparently divergent conclusions are obtained on the impact of various factors (delay and inverter response time) on these control interactions.

Using a detailed small signal model of two PV plants connected to a realistic 45 km long 27.6 kV feeder in Ontario, the impact of slope of Volt-Var function, delay, response time of current controller, system strength, and X/R ratio of feeder on the controller interaction, are investigated. The results of small signal studies are validated using time domain simulation studies.

The PV plants interact adversely with increase in slope, increase in X/R ratio, and reduction in system strength. With increase in delay, and response time, the sensitive eigenvalue moves towards the right and make the system unstable. However, with further increase, this sensitive eigen value shifts left, and thus make system stable. This observation shows that the increase in delay and response time can have both a positive or negative impact on the interaction between PV plants. Thus, the impact of delay, and response time on system stability should be analyzed on system by system basis to ensure stable operation.

BIBLIOGRAPHY

- [1] "United Nations Framework Convention On Climate Change :-Doha amendment to the Kyoto Protocol ", United Nations, 2013.
- [2] S. Lacey. (2018, 5 Nov). *Global Solar Demand Monitor: Q2 2017*.
- [3] "Common Functions for Smart Inverters 4th Edition," EPRI, Product Id: 3002008217, California, Dec. 2016.
- [4] "Demonstration of Essential Reliability Services by a 300 MW Solar Photovoltaic Power Plant," NREL, Product ID: NREL/TP-5D00-67799, 2017.
- [5] "IEEE Standard for Interconnection and Interoperability of Distributed Energy Resources with Associated Electric Power Systems Interfaces," *IEEE Std 1547-2018*, pp. 1-138, 2018.
- [6] "Rule 21: -Generating Facility Interconnections," Southern California Edison, July 2014.
- [7] S. Chakraborty, A. Hoke and B. Lundstrom, "Evaluation of multiple inverter volt-VAR control interactions with realistic grid impedances," in *2015 IEEE PES GM*, 2015, pp. 1-5.
- [8] M. G. Kashani, Y. Cho and S. Bhattacharya, "Design consideration of volt-VAR controllers in distribution systems with multiple PV inverters," in *2016 IEEE ECCE*, 2016, pp. 1-7.
- [9] S. Chakraborty, A. Nelson and A. Hoke, "Power hardware-in-the-loop testing of multiple photovoltaic inverters' volt-var control with real-time grid model," in *2016 ISGT*, 2016, pp. 1-5.
- [10] H. Li, J. Smith and M. Rylander, "Multi-Inverter Interaction with Advanced Grid Support Functions," in *CIGRE US National Committee 2014 Grid of the Future Symposium*, 2014, pp. 1-6.
- [11] A. Mahendra, "Novel Control of PV Solar and Wind Farm Inverters as STATCOM for Increasing Connectivity of Distributed Generators," MESC thesis, Western University, Canada, 2013.
- [12] M. Liserre, F. Blaabjerg and S. Hansen, "Design and Control of an LCL-Filter-Based Three-Phase Active Rectifier," *IEEE Trans. on Industry Applications*, vol. 41, pp. 1281-1291, 2005.
- [13] S. Soni, "Solar PV Plant Model Validation for Grid Integration Studies," MESC Thesis, Arizona State University, USA, 2014.
- [14] N. Pogaku, M. Prodanovic and T. C. Green, "Modeling, Analysis and Testing of Autonomous Operation of an Inverter-Based Microgrid," *IEEE Trans. on Power Electronics*, vol. 22, pp. 613-625, 2007.
- [15] A. Yazdani and R. Iravani, *Voltage Sourced Converters in Power Systems Modeling, Control and Applications*. New York: IEEE Press/Wiley, 2010.